Bioactive Materials 6 (2021) 3288–3299

Contents lists available at ScienceDirect

Bioactive Materials

journal homepage: www.sciencedirect.com/journal/bioactive-materials

L-cysteine-modified chiral gold nanoparticles promote periodontal tissue regeneration

Shuang Zhang [a,1], Hong Zhou [b,1], Na Kong [c], Zezheng Wang [a], Huangmei Fu [c], Yangheng Zhang [a], Yin Xiao [d,e,***], Wenrong Yang [c,**], Fuhua Yan [a,e,*]

[a] Nanjing Stomatological Hospital, Medical School of Nanjing University, Nanjing, Jiangsu, People's Republic of China
[b] Key Laboratory of Optic-electric Sensing and Analytical Chemistry for Life Science, MOE; College of Chemistry and Molecular Engineering, Qingdao University of Science and Technology, Qingdao, 266042, People's Republic of China
[c] School of Life and Environmental Science, Centre for Chemistry and Biotechnology, Deakin University, Geelong, VIC, Australia
[d] Institute of Health and Biomedical Innovation, Queensland University of Technology, Brisbane, Queensland, 4059, Australia
[e] Australia-China Centre for Tissue Engineering and Regenerative Medicine, Queensland University of Technology, Australia

ARTICLE INFO

Keywords:
Chirality
Gold nanoparticles
Periodontal
Tissue regeneration
Autophagy

ABSTRACT

Gold nanoparticles (AuNPs) with surface-anchored molecules present tremendous potential in tissue regeneration. However, little is known about chiral-modified AuNPs. In this study, we successfully prepared L/D-cysteine-anchored AuNPs (L/D-Cys-AuNPs) and studied the effects of chiral-modified AuNPs on osteogenic differentiation and autophagy of human periodontal ligament cells (hPDLCs) and periodontal tissue regeneration. *In vitro*, more L-Cys-AuNPs than D-Cys-AuNPs tend to internalize in hPDLCs. L-Cys-AuNPs also significantly increased the expression of alkaline phosphatase, collagen type 1, osteocalcin, runt-related transcription factor 2, and microtubule-associated protein light chain 3 II and decreased the expression of sequestosome 1 in hPDLCs compared to the expression levels in the hPDLCs treated by D-Cys-AuNPs. *In vivo* tests in a rat periodontal-defect model showed that L-Cys-AuNPs had the greatest effect on periodontal-tissue regeneration. The activation of autophagy in L-Cys-AuNP-treated hPDLCs may be responsible for the cell differentiation and tissue regeneration. Therefore, compared to D-Cys-AuNPs, L-Cys-AuNPs show a better performance in cellular internalization, regulation of autophagy, cell osteogenic differentiation, and periodontal tissue regeneration. This demonstrates the immense potential of L-Cys-AuNPs for periodontal regeneration and provides a new insight into chirally modified bioactive nanomaterials.

1. Introduction

Periodontitis is not only a major cause of tooth loss in adults [1] but also causes systemic inflammatory burden and other systemic disorders [2]. Human periodontal ligament cells (hPDLCs) are thought to be multipotent and a potential applicable cell source for successful regeneration of periodontal tissue [3]. In addition, hPDLCs are heterogeneous cell populations with cell differentiation capacity that need to be functionally regulated in periodontal regeneration. Recently, the development of nanotechnology has brought forth a series of promising regenerative medicines, including those based on polymeric and inorganic nanoparticles. Among the successful nanoparticles, gold nanoparticles (AuNPs) that possess many unique and excellent characteristics have been extensively studied for biomedical applications [4], such as promotion of cell mineralization and osteogenic differentiation [5]. For example, the effect of AuNPs on stem-cell osteogenic differentiation has been reported [6]. Previous work conducted by our team has also

Peer review under responsibility of KeAi Communications Co., Ltd.

* Corresponding author. Nanjing Stomatological Hospital, Medical School of Nanjing University, 30 Zhongyang Road, Nanjing, Jiangsu, 210008, People's Republic of China.

** Corresponding author. School of Life and Environmental Sciences, Centre for Chemistry and Biotechnology, Deakin University, 75 Pigdons Road, Geelong, Victoria, 3217, Australia.

*** Corresponding author. Institute of Health and Biomedical Innovation & the Australia-China Centre for Tissue Engineering and Regenerative Medicine, Queensland University of Technology, Brisbane, Queensland, 4059, Australia.

E-mail addresses: yin.xiao@qut.edu.au (Y. Xiao), wenrong.yang@deakin.edu.au (W. Yang), yanfh@nju.edu.cn (F. Yan).

[1] These authors contributed equally.

https://doi.org/10.1016/j.bioactmat.2021.02.035
Received 17 December 2020; Received in revised form 17 February 2021; Accepted 24 February 2021
Available online 13 March 2021

Abbreviations

AuNPs	gold nanoparticles
L/D-Cys-AuNPs	L/D-cysteine anchored AuNPs
hPDLCs	human periodontal ligament cells
H_2S	hydrogen sulfide
–SH	mercapto group
$HAuCl_4$	tetrachloroauric acid
UV–vis	ultraviolet–visible
DLS	dynamic light scattering
TEM	transmission electron microscopy
CD	circular dichroism
DMEM	dulbecco's modified eagle medium
FBS	fetal bovine serum
3-MA	3-methyladenine
CCK-8	Cell Counting Kit-8
ICP-MS	inductively coupled plasma mass spectrometry
PBS	phosphate buffered saline
ALP	alkaline phosphatase
ARS	alizarin red S
qRT-PCR	quantitative real time polymerase chain reaction
GAPDH	glyceraldehyde-3-phosphate dehydrogenase
WB	western blot
RUNX2	runt-related transcription factor 2
LC3	microtubule-associated protein light chain 3
COL1	collagen type I
OCN	osteocalcin
SQSTM1	sequestosome 1
SPF	specific-pathogen free
μCT	Micro-computed tomography
BMD	bone mineral density
TV	tissue volume
BV	bone volume
Tb.Th	trabecular thickness
Tb.N	trabecular number
EDTA	ethylene diamine tetraacetic acid
H&E	hematoxylin and eosin
VG	Van Gieson's
IHC	immunohistochemistry
LSPR	localized surface plasmon resonance
NAB	newly-formed alveolar bones
NPDL	newly-formed periodontal ligaments
L(D)-PAV	poly (acryloyl-L(D)-valine)
MSCs	mesenchymal stem cells
SD	Sprague-Dawley

proposed size-dependent effects of AuNPs on the extent of osteogenic differentiation of human periodontal ligament progenitor cells [5]. Despite the extensive efforts in this field to date, the application of AuNPs still needs better design and specific targeting of the molecular pathways to guide cell differentiation.

Chirality is a distinctive biochemical signature of life [7]. All amino acids (except glycine) in proteins are left-handed (L-form), whereas all sugars in DNA and RNA are right-handed (D-form) [8]. Chirality is important in materials science and medical technology. In materials science, the exploration of the material properties and molecular functions on the basis of chirality controls is a scientifically elegant approach [9]. These explorations include chiral materials [10], analyses of chiral structures [11], basic physical chemistry [12], chiral plasmons and optics [13], chirality-controlled catalysis and synthesis [14], chiral recognition [15], and chiral separation [9,16]. In medical technology, plasmon-enhanced chiral signals may have immense potential in the detection and treatment of diseases [17]. For example, monitoring the cell internalization of nanoparticles [18], specific microRNA detection [19], detection of Parkinson's disease [20], and photosensitizing in photodynamic therapy [17,21]. Therefore, we designed this research on the basis of the general importance of chirality.

Cysteine is a common sulfur-containing amino acid in the human body [22] and plays an essential role in protein synthesis, detoxification, and metabolism. Cysteine deficiency can result in a number of diseases, including loss of muscle and fat, skin lesions, Parkinson's disease, Alzheimer's disease, and acquired immune deficiency syndromes [23]. Hydrogen sulfide (H_2S) can be synthesized from cysteine to promote osteogenic differentiation of hPDLCs [24]. Among the amino acids found in the proteins of human body, cysteine is the one that contains a mercapto group (–SH). AuNPs can be combined with –SH groups through Au-S bonding [25]. We have recently demonstrated electrochemical evidence of chiral molecule recognition using L/D-cysteine-modified gold electrodes [26] and developed an ultrasensitive detection method for chiral molecules of L/D-carnitine using L/D-cysteine-modified AuNPs (L/D-Cys-AuNPs) [27]. Ding et al. previously investigated the adhesion and differentiation of stem cells on L- or D-cysteine-modified Au-sputtered glass substrates [28]. These results confirmed that chiral molecules can influence cellular behavior during adhesion and differentiation. A recent study proved that osteogenic differentiation of mesenchymal stem cells was not affected by poly (acryloyl-D-valine)-AuNPs but was significantly promoted by poly (acryloyl-L-valine)-AuNPs [8]. L-ascorbic acid was also reported to decrease external symptoms of burn injury of damaged epidermis and was used commercially [29].

Autophagy is regarded as an important aspect of nanoparticles for modulating osteogenic differentiation [5] and is furthermore induced in some osteogenic differentiation processes [30,31]. Pharmacological activation of autophagy significantly increases osteoblast-differentiation activity and restores bone volume [31], while the deletion of autophagy-related components can inhibit osteoblast differentiation [32]. Many nanoscale inducers of autophagy with various sizes and/or morphologies have been developed. For example, it was demonstrated that chiral nanomaterials with different configurations selectively activate autophagy in cells [33]. Although some appreciable progress has been made, the effects of chiral surface molecules and the related control of autophagy still require major clarification. Although chirality is ubiquitous in nature, the application of chiral surface molecules in the design of biomaterials is seldom investigated. In this study, we investigated whether L/D-Cys-AuNPs can regulate the osteogenic differentiation of hPDLCs and subsequently stimulate periodontal regeneration through autophagy.

2. Materials and methods

Synthesis of L/D-Cys-AuNPs. Bare AuNPs with a diameter of about 45 nm were synthesized using a chemical reduction method from tetrachloroauric acid ($HAuCl_4$), as reported earlier [27,34,35]. Briefly, 1 mL of 5×10^{-3} M $HAuCl_4 \cdot 3H_2O$ solution was added to 18 mL of boiling deionized water with stirring. With stirring and heating, 0.365 mL of 0.5% w/w sodium citrate was added to reduce the $HAuCl_4$. After the color was noticeably changed to wine red, the heating was maintained for another 10 min and then stopped. The stirring was continued until the solution cooled to approximately 25 °C. Thereafter, deionized water was added to the final solution to reach a volume of 20 mL, giving a final concentration of the AuNP solution of 2.5×10^{-4} M.

The L/D-Cys-AuNPs were prepared as follows [27,34,36]. First, 0.1

mL of 1 × 10^{-4} M L/D-cysteine solutions were added to 5 mL of the AuNP solution, followed by 2 h of stirring, before centrifuging the L/D-Cys-AuNP solutions. After centrifugation, the supernatants were removed. The precipitates were dispersed in deionized water by sonication. All reagents used to synthesize the L/D-Cys-AuNPs were purchased from Sigma-Aldrich Co. (St Louis, Missouri, USA).

Characterization of L/D-Cys-AuNPs. Ultraviolet–visible (UV–vis) spectrometry (SpectraMax M3 Microplate Spectrophotometer, Molecular Devices, Sunnyvale, CA, USA), dynamic light scattering (DLS; Nano-ZS, Malvern Panalytical Ltd, Malvern, United Kingdom), zeta potential measurements (Nano-ZS, Malvern Panalytical Ltd, Malvern, United Kingdom), transmission electron microscopy (TEM; JEOL-2100F, JEOL, Akishima city, Tokyo, Japan), and circular dichroism analysis (CD; Chirascan Spectrometer, Applied Photophysics Ltd, Leatherhead, Surrey, United Kingdom) were used to characterize the synthesized AuNPs and L/D-Cys-AuNPs.

Cell culture. hPDLCs were purchased from ScienCell Research Laboratories (Carlsbad, California, USA). Cells from passages two to six were used in our experiments. The normal cell-culture growth medium consisted of Dulbecco's modified eagle medium (DMEM; Gibco cell culture; Thermo Fisher Scientific, Waltham, Massachusetts, USA), 10% fetal bovine serum (FBS; ScienCell Research Laboratories), and 1% streptomycin/penicillin (HyClone, Logan, Utah, USA). The osteogenic differentiation medium consisted of the growth medium, 10 mM β-glycerophosphate (Sigma-Aldrich Co.), 0.28 μM L-ascorbic acid (Sigma-Aldrich Co.), and 0.1 μM dexamethasone (Sigma-Aldrich Co.). In autophagy inhibition experiments, 5 mM of 3-methyladenine (3-MA, Sigma-Aldrich Co.) was also used. During testing, the culture medium was replaced twice a week.

Cell viability and proliferation assay. Cell Counting Kit-8 (CCK-8; Dojindo Molecular Technologies, Shangyi city, Kumamoto prefecture, Japan) was used to determine the viability and proliferation of hPDLCs. The cells were seeded on the bottom of 96-well plates at a density of 4.0×10^3 cells/well. After the cells reached 70–80% confluence, L/D-Cys-AuNP solution at an Au concentration of 10 μM was added as reported earlier [5]. Then, at 1, 3, 5, and 7 days, the CCK-8 reagent was added to each well at 10% of the total volume. After incubation for 160 min, a SpectraMax M3 Microplate Spectrophotometer (Molecular Devices, Sunnyvale, CA, USA) was used to measure the optical density of each well at a wavelength of 450 nm.

TEM. TEM (HT7700; Hitachi Ltd., Tokyo, Japan) was used to observe the L/D-Cys-AuNPs internalized by hPDLCs. The cells were cultured in the growth medium at an initial density of 2.0×10^5 cells/well in 6-well plates. When the cells reached 70–80% confluence, L/D-Cys-AuNPs were added. After 3 days of incubation, the cells were fixed, dehydrated, embedded, cut, and then observed by TEM.

Inductively coupled plasma mass spectrometry (ICP-MS). ICP-MS (ICAP7400, Thermo Fisher Scientific) was used to detect the quantity of the two types of AuNPs in or on the hPDLCs. hPDLCs were seeded into 100-mm-diameter dishes at a density of 1.5×10^6 cells/dish. When the cells reached 70–80% confluence, the growth medium was replaced by the osteogenic differentiation medium with L/D-Cys-AuNPs. After 3 days, the dishes were washed five times with phosphate buffered saline (PBS; HyClone, Logan, Utah, USA) to remove the free floating AuNPs. The cells were then harvested and counted. The harvested cells were dissolved with aqua regia, diluted, and measured *via* ICP-MS to determine Au concentrations.

Alkaline phosphatase (ALP) activity. hPDLCs were seeded into 12-well plates at a density of 1.0×10^5 cells/well. When the cells achieved 70–80% confluence, the growth medium was replaced by the osteogenic differentiation medium. Meanwhile, L/D-Cys-AuNPs were added. On days 3, 5 and 7, the ALP Assay Kit (Beyotime Institute of Biotechnology, Shanghai, China) was used to measure the ALP activity of the cells. hPDLCs were washed three times, lysed, and centrifuged to collect the supernatant. After diluting, 50 μL of the supernatant and 50 μL of para-nitrophenyl phosphate solution were mixed in a 96-well plate. The plates were then incubated under dark conditions at 37 °C for 30 min. Thereafter, 100 μL of the stop solution was added, and the absorbance was measured at a wavelength of 405 nm.

ALP staining. hPDLCs were cultured and treated as described in the ALP assay outlined above. On day 7, the cells were washed and fixed. Subsequently, the BCIP/NBT ALP staining kit (Beyotime Institute of Biotechnology, Shanghai, China) was used according to the manufacturer's instructions. The ALP staining results were observed using an inverted optical microscope (IMT-2; Olympus Corporation, Tokyo, Japan) and photographed using a digital camera (Canon EOS 70D, Tokyo, Japan).

Alizarin red S (ARS) staining and quantification. The cells were cultured and treated as described for the ALP assay. On day 21, the cells were washed, fixed, and stained with 2% ARS staining solution (Sigma-Aldrich Co.). The ARS staining results were observed and photographed as outlined in the ALP staining procedure. The ARS was quantified using 10% (w/v) cetylpyridinium chloride (Sigma-Aldrich Co.). After the stained mineral deposition was desorbed, the absorbance at a wavelength of 562 nm was measured.

Von Kossa staining and quantification. The cells were cultured and treated as described for the ARS assay. The cells were fixed and stained with 5% silver nitrate (Sigma-Aldrich Co.) under ultraviolet light. Then, the cells were treated with 10% sodium thiosulphate (Sigma-Aldrich Co.) for 5 min. The quantification was performed using ImageJ software (National Institutes of Health, USA).

Quantitative real-time polymerase chain reaction (qRT-PCR). hPDLCs were seeded into 6-well plates at a density of 2.0×10^5 cells/well and left to proliferate until reaching 70–80% confluence. The medium was then changed to the osteogenic differentiation medium, and L/D-Cys-AuNPs were added. After 3, 5, and 7 days of culturing, the total mRNA was obtained using an RNA extraction kit (Tiangen, Beijing, China). The mRNA was reverse-transcribed into cDNA using the PrimeScript™ RT Reagent Kit (Takara Bio, Otsu, Japan). The cDNA samples were amplified by qRT-PCR according to the primer sequences listed in our previous study [5] and normalized to the housekeeping gene glyceraldehyde-3-phosphate dehydrogenase (GAPDH).

Western blot (WB) tests. The cells were cultured and treated as described for the qRT-PCR assay. On day 7, cell lysis buffer for Western and IP (Beyotime Institute of Biotechnology, Shanghai, China) together with phenylmethanesulfonyl fluoride (Beyotime Institute of Biotechnology, Shanghai, China) were used to extract the protein. After quantification, the protein was loaded and ran in sodium dodecyl sulfate polyacrylamide gel, and then transferred onto membranes. The blocked membranes were incubated with the primary antibodies (ALP; Santa Cruz Biotechnology, Inc., Dallas, Texas, USA), runt-related transcription factor 2 (RUNX2; Cell Signaling Technology Inc., Danvers, MA, USA), microtubule-associated protein light chain 3 (LC3; Cell Signaling Technology Inc., Danvers, MA, USA), collagen type I (COL1; Abcam, Cambridge, MA, USA), osteocalcin (OCN; Affinity Biosciences, Cincinnati, OH, USA), sequestosome 1 (SQSTM1; Proteintech, Manchester, M3 3WF, United Kingdom), and GAPDH (KeyGEN BioTECH Corp., Ltd, Nanjing, Jiangsu, China). GAPDH was used as an internal control. After washing four times, the membranes were incubated with secondary antibodies for 2 h. Immunoreactive bands were detected using the developer (KeyGEN BioTECH Corp., Ltd) and visualized using a G:BOX chemiXR5 imaging system (Syngene International Ltd, Bangalore, Karnataka, India). The band intensity was quantified using ImageJ software (National Institutes of Health, USA).

Construction of tissue-engineered compound. A resorbable collagen membrane (Geistlich Bio-Gide®; Geistlich, Wolhusen, Lucerne, Switzerland) was trimmed under aseptic conditions and placed into 24-well plates with the rough face up. Thereafter, hPDLCs were seeded onto the rough face at a density of 1.0×10^4 cells/membrane. After being cultured in the growth medium overnight, the cell-membrane compounds were cultured for 3 days in the medium without AuNPs, with L-Cys-AuNPs or with D-Cys-AuNPs.

Rat periodontal fenestration defect model. All the animal experiments obeyed the rules of the National Institutes of Health guide for the care and use of Laboratory animals and were approved by the Animal Ethics Committee of Nanjing University. We confirm authors' compliance with all relevant ethical regulations. This model was modified from a periodontal-defect model reported previously [37]. All model-making procedures were performed under anesthesia induced by intraperitoneal injection (0.3 mL/100 g body weight) of 2% (w/v) sodium pentobarbital (Lan Tai Chem, Beijing, China), supplemented by 5% (w/v) atropine sulfate (Wuhu Kangqi Pharmaceutical Co., Ltd., Wuhu, Anhui, China). Eighteen male Sprague-Dawley (SD) rats with a known specific-pathogen free (SPF) status at 7 weeks old were purchased from Sino-British SIPPR/BK Lab. Animal Ltd. (Shanghai, China). The rats were raised in SPF conditions with a 12 h dark and 12 h light cycle. The food and water were sterilized and constantly available. After acclimatization for 1 week, the experiments were applied under anesthesia and sterilized conditions. Briefly, an extra-oral full thickness incision parallel to the lower border of the right mandible was made. A mucoperiosteal flap was subsequently elevated to expose the buccal surface of mandibular. The alveolar bone covering the root surfaces of the molars was removed using dental burs at a low speed under copious normal saline irrigation. The defect was approximately 5 mm in length, 2 mm in width and 1.2 mm in depth. The periodontal ligament tissues and cementum in this area were removed by a sharp curette. The flap was repositioned and sutured. The tissue-engineered compound was adapted to the defect using the cell side facing the denuded root surface. Defects with the hPDLCs cultured in growth medium without AuNPs were used as controls. A bioresorbable matrix barrier membrane (Sunstar Americas, Chicago, Illinois, USA) was then used to cover the tissue-engineered compound to exclude the overlying connective tissue from the defect. The flap was repositioned and sutured in layers. The rats were sacrificed 3 weeks after the surgery using excessive inhalation of isoflurane (RWD Life Science Co., Ltd, Shenzhen, Guangdong, China). The mandibles ($n = 6$ for each group) were harvested and fixed in 4% paraformaldehyde solution (Servicebio, Wuhan, Hubei, China).

Micro-computed tomography (μCT) analysis. The mandibular bone specimens were scanned using a μCT scanner (QuantumGX; PerkinElmer, Tokyo, Japan) at a pixel size of 18 μm, a voltage of 90 kV, and a current of 80 μA. The scanning provided 360° rotation over the course of 14 min and a scanning field of 9 mm × 9 mm × 9 mm. The images, bone mineral density (BMD), tissue volume (TV), bone volume (BV), trabecular thickness (Tb.Th), and trabecular number (Tb.N) were obtained from the scans with the μCT system software.

Histology analysis and histomorphometric measurements. Following μCT analysis, all specimens were rinsed and decalcified in ethylene diamine tetraacetic acid (EDTA; Yonghua chemical technology (Jiangsu) Co., Ltd., Changshu, Jiangsu, China) solution with regular solution changes every 3–7 days, until the bone tissues could be easily penetrated by a syringe. Then, the specimens were embedded using paraffin. The specimens were sectioned to a thickness of 3–4 μm using a microtome (Leica Microsystems, Shanghai, China). The sections were stained with hematoxylin and eosin (H&E) staining, Masson staining, Van Gieson's (VG) picrofuchsin staining and Goldner's trichome staining. The stained slides were scanned using a NanoZoomer-S60 digital slide scanner (Hamamatsu Photonics, Hamamatsu, Shizuoka, Japan) for subsequent analysis. The percentages of new alveolar bone or new periodontal ligament formation were calculated as the area of new alveolar bone or new periodontal ligament divided by the total defect area.

Immunohistochemistry (IHC) analysis. Immunohistochemical staining was applied in accordance to the following procedure: dewaxing, hydration, and neutralization of endogenous peroxidase activity. The primary antibodies were LC3 and SQSTM1 (both from Servicebio).

Statistical analysis. Data are shown as mean ± standard deviation. Comparisons were performed *via* one-way analysis of variance using IBM SPSS Statistics software 24.0. Statistical significance (two-tailed) was identified as compared with a control group $P < 0.05$ (marked as *), $P < 0.01$ (marked as **), and $P < 0.001$ (marked as ***). In the case of the comparison between groups: $P < 0.05$ (marked as #), $P < 0.01$ (marked as ##), and $P < 0.001$ (marked as ###).

3. Results

Design and synthesis of chiral AuNPs. The TEM results confirmed that the AuNPs, L-Cys-AuNPs, and D-Cys-AuNPs were approximately spherical (Fig. 1A). The DLS results indicated that the average hydration diameters of AuNPs, L-Cys-AuNPs, and D-Cys-AuNPs were all approximately 45 nm (Fig. 1B). The two types of Cys-AuNPs (L-Cys-AuNPs and D-Cys-AuNPs) clearly showed different chirality. Fig. 1C shows the essential mirror-image CD profiles of the synthesized AuNPs. As seen in Fig. 1D, the UV–vis absorption profile of L/D-Cys-AuNPs had a localized surface plasmon resonance (LSPR) peak at approximately 530 nm. No significant red-shift and no peak broadening were observed in the LSPR peaks of L and D-Cys-AuNPs compared to that of bare AuNPs, which supported better dispersion in the medium. Fig. 1E shows that the average zeta potential values of bare AuNPs, L-Cys-AuNPs, and D-Cys-AuNPs were −32.4, −20.4, and −19.4 mV, respectively. The cysteine-modified AuNPs exhibited significantly larger zeta potential values than that of bare AuNPs.

Cell differentiation after treatment with chiral AuNP. Compared with the control group, L/D-Cys-AuNPs had almost no influence on the morphology of hPDLCs on day 3 (Fig. 2A). All the groups exhibited an increase in the number of cells. The CCK-8 assay (Fig. 2B) revealed that on days 3 and 5, the L-Cys-AuNPs and D-Cys-AuNPs both promoted cell viability and proliferation of hPDLCs compared to the control group. L/D-Cys-AuNPs resulted in no detrimental effects on cell morphology, viability, or proliferation, indicating that L/D-Cys-AuNPs showed desirable cytocompatibility at an Au concentration of 10 μM.

The uptake and localization of the AuNPs in hPDLCs were demonstrated by TEM and ICP-MS. In the L/D-Cys-AuNP-treated groups (Fig. 2C), AuNPs appeared in the cytoplasm, particularly in some intracellular vesicles such as autophagosomes. Furthermore, it was noted that no AuNPs were found in the mitochondria or nucleus. The ICP-MS results (Fig. 2D) confirmed that there were AuNPs present in the hPDLCs and the amount of L-Cys-AuNPs was significantly higher than that of the D-Cys-AuNPs.

Both L-Cys-AuNPs and D-Cys-AuNPs enhanced the ALP activities of hPDLCs on day 3 and day 7. Interestingly, on day 5 only L-Cys-AuNPs significantly raised the ALP activity. Compared to D-Cys-AuNPs, L-Cys-AuNPs exerted a more significant influence on ALP activity on days 3, 5, and 7 (Fig. 2E). On day 7, the ALP staining showed a similar trend as seen with the ALP activity (Fig. 2F). Subsequently, the mineralization ability of hPDLCs was observed with ARS and von Kossa on day 21. The hPDLCs cultured with L-Cys-AuNPs showed significantly greater mineral deposition than the cells cultured with a control solution and D-Cys-AuNPs (Fig. 2G).

On day 5, all the tested osteogenic gene levels measured by qRT-PCR including those of *ALP*, *COL1*, *OCN* and *RUNX2* in the L-Cys-AuNP group were significantly higher than those in both the control and D-Cys-AuNPs group (Fig. 3A).

To further study the influence of the change in the levels of osteogenic genes, the protein expression levels of these genes were measured by WB on day 7. The levels of the ALP, COL1, OCN and RUNX2 proteins in the L-Cys-AuNP group were significantly higher than those in both the control and D-Cys-AuNP groups (Fig. 3B).

L/D-Cys-AuNP-induced autophagy in hPDLCs. Because L/D-Cys-AuNPs were internalized in autophagosomes, some of the autophagy genes and proteins were further examined. On day 3, the mRNA levels of *LC3* in the L-Cys-AuNP group were significantly higher than those in the D-Cys-AuNP group (Fig. 4A). On day 5, the presence of L-Cys-AuNPs increased the mRNA levels of beclin1 (*BECN1*) in the hPDLCs, and these

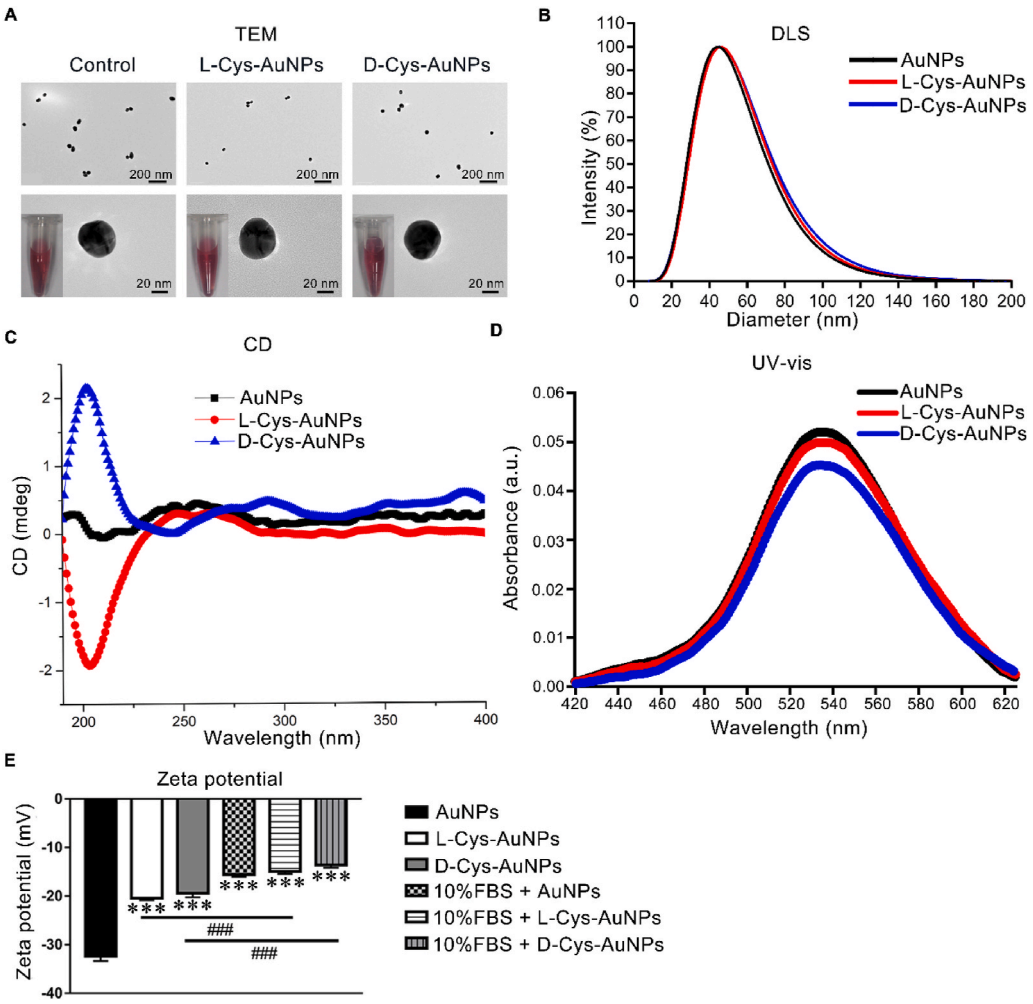

Fig. 1. Characterization of bare AuNPs, L-Cys-AuNPs, and D-Cys-AuNPs. (A) TEM images. Inset: corresponding photographs. (B) DLS images. (C) CD spectra. (D) UV–vis absorption spectra. (E) Zeta potential of the samples in water and 10% FBS. ***$P < 0.001$ compared with the control group, ###$P < 0.001$.

levels were significantly higher than those in the D-Cys-AuNP group (Fig. 4A). On day 7, the mRNA levels of *BECN1* in hPDLCs cultured with L-Cys-AuNPs were higher than those in the D-Cys-AuNPs. L-Cys-AuNPs also increased the mRNA levels of *LC3* in hPDLCs on day 7. A significant difference was observed between the effects of L-Cys-AuNPs and D-Cys-AuNPs on hPDLCs at this timepoint (Fig. 4A).

Autophagy-related proteins including LC3 and SQSTM1 were detected by WB on day 7. As shown in Fig. 4B, the levels of LC3-II in the L-Cys-AuNP group were significantly higher than those in the D-Cys-AuNP group. The SQSTM1 levels in the L-Cys-AuNP group were significantly lower than those in the D-Cys-AuNP group.

Effects of L/D-Cys-AuNPs *via* the regulation of autophagy. We used an autophagy inhibitor, 3-MA, to further confirm the effects of autophagy by L/D-Cys-AuNPs on different levels of osteogenesis. Fig. 4C and D show that the osteoinduction effect of L-Cys-AuNPs was blocked when 3-MA was added.

L-Cys-AuNPs showed better periodontal regeneration potential. The μCT analysis (Fig. 5A) showed that there was more bone regeneration in the L-Cys-AuNP-treated group than that in the D-Cys-AuNP-treated and control groups. In Fig. 5B, the BMD, BV, BV/TV, Tb.N, and Tb.Th results all revealed that tissue-engineered compounds treated with L-Cys-AuNPs had more favorable bone regeneration capacity than those treated with D-Cys-AuNPs and the control group. Greater amounts of newly-formed alveolar bones (NAB) and newly-formed periodontal ligaments (NPDL) were found in the L-Cys-AuNP-treated group (Fig. 5C). Specimen sections stained with H&E, Masson, Goldner's trichome, and VG stains were observed (Fig. 5D). The amount of NAB was evaluated by Masson and Goldner's trichome staining [38]. The effects on regeneration of periodontal ligaments were evaluated by VG staining [39]. The L-Cys-AuNP-treated group showed the deepest reddish orange stain by VG staining, indicating that the L-Cys-AuNP-treated group formed the largest number of NPDL.

L/D-Cys-AuNP-modulated autophagic potential *in vivo*. Immunohistochemistry images (Fig. 6A) and the quantitative image analysis (Fig. 6B) showed a difference in autophagy as related to LC3 and SQSTM1 protein expression among the groups.

4. Discussion

Although the use of biomaterials is extensive, and chirality is ubiquitous, the combination of the two is seldom investigated and can facilitate the development and application of chiral biomaterials. The relationship between chiral AuNPs and osteogenesis is still unknown, in addition to its underlying mechanism.

We designed and synthesized AuNPs with surface-anchored chiral amino acids (L/D-cysteine). The characterization results of the D-Cys-AuNPs and L-Cys-AuNPs were similar, except for the CD results, where the two enantiomers showed essential mirror-image CD spectra.

As the AuNPs are non-degradable inorganic metal nanoparticles [40], their amounts and distribution in cells are interesting to analyze. We quantified the amounts of L/D-Cys-AuNPs inside or tightly bound on the cytomembrane of the hPDLCs by ICP-MS. The results showed that

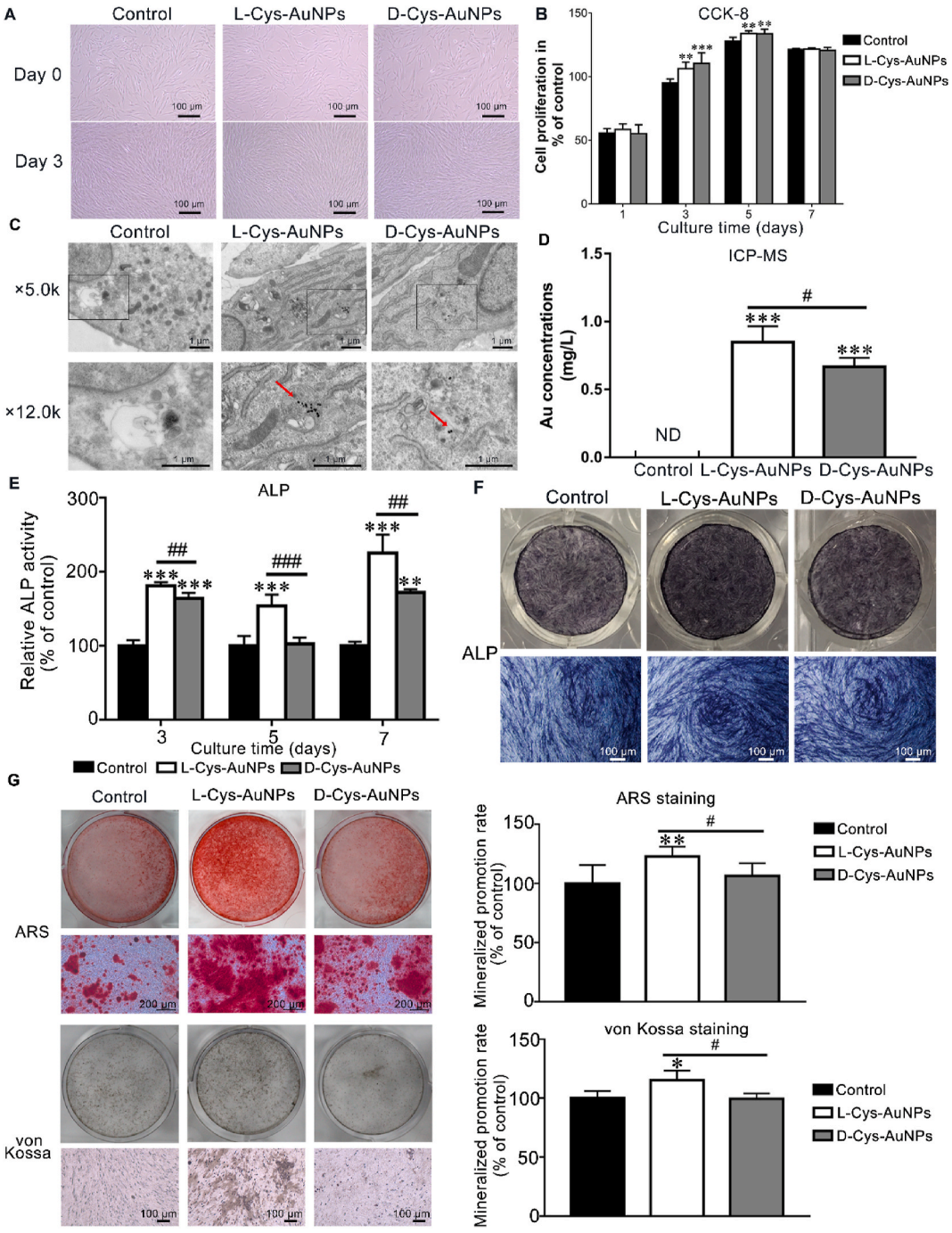

Fig. 2. Biocompatibility, uptake, cellular localization, ALP activity, and mineral deposition of L/D-Cys-AuNPs. hPDLCs were cultured with AuNPs. (**A**) Light microscopy images of hPDLCs before and after treatment with different types of AuNPs for 3 days. (**B**) Effects of AuNPs on cell viability and proliferation of hPDLCs on days 1, 3, 5, and 7. (**C**) TEM images of hPDLCs incubated with AuNPs on day 3. The arrows indicate the internalized AuNPs. (**D**) Concentrations of Au on day 3. ND means not detected. (**E**) ALP activity levels on days 3, 5, and 7. (**F**) ALP staining on day 7. (**G**) ARS and von Kossa staining and quantification of mineral deposition on day 21. $^{*}P < 0.05$, $^{**}P < 0.01$, $^{***}P < 0.001$ compared with the control group, $\#P < 0.05$, $\#\#P < 0.01$, $\#\#\#P < 0.001$.

the amount of L-Cys-AuNPs was significantly higher than that of D-Cys-AuNPs, suggesting that chirality can influence the cellular internalization of nanoparticles. Deng et al. previously reported the effect of chirality on the cellular uptake at the nanoscale. They grafted poly (acryloyl-L(D)-valine) (L(D)-PAV) chiral molecules onto the surface of AuNPs [41]. The intracellular accumulation of L-PAV-AuNPs was higher than that of D-PAV-AuNPs in mesenchymal stem cells (MSCs), which is in accordance with our findings [8]. In another study, they reported that A549 and HepG2 cells internalized significantly larger amount of D-PAV-AuNPs than L-PAV-AuNPs [41], which is different from our results. This may be because we used different cells (A549 and HepG2 vs hPDLCs), different diameters of AuNPs (approximately 16 nm in their case and approximately 45 nm in this study) and different modified molecular (PAV vs Cys). Because the adhesion and internalization of the NPs occur simultaneously, it is difficult to study the adhesion of AuNPs to hPDLCs. According to previous studies [8,41], it is possible that upon contact with serum, the Cys-AuNPs may be rapidly covered by the serum proteins, forming a biomolecular corona that interacts with the cell membrane, resulting in internalization *via* endocytosis. We propose that the hPDLCs internalized more L-Cys-AuNPs than D-Cys-AuNPs because

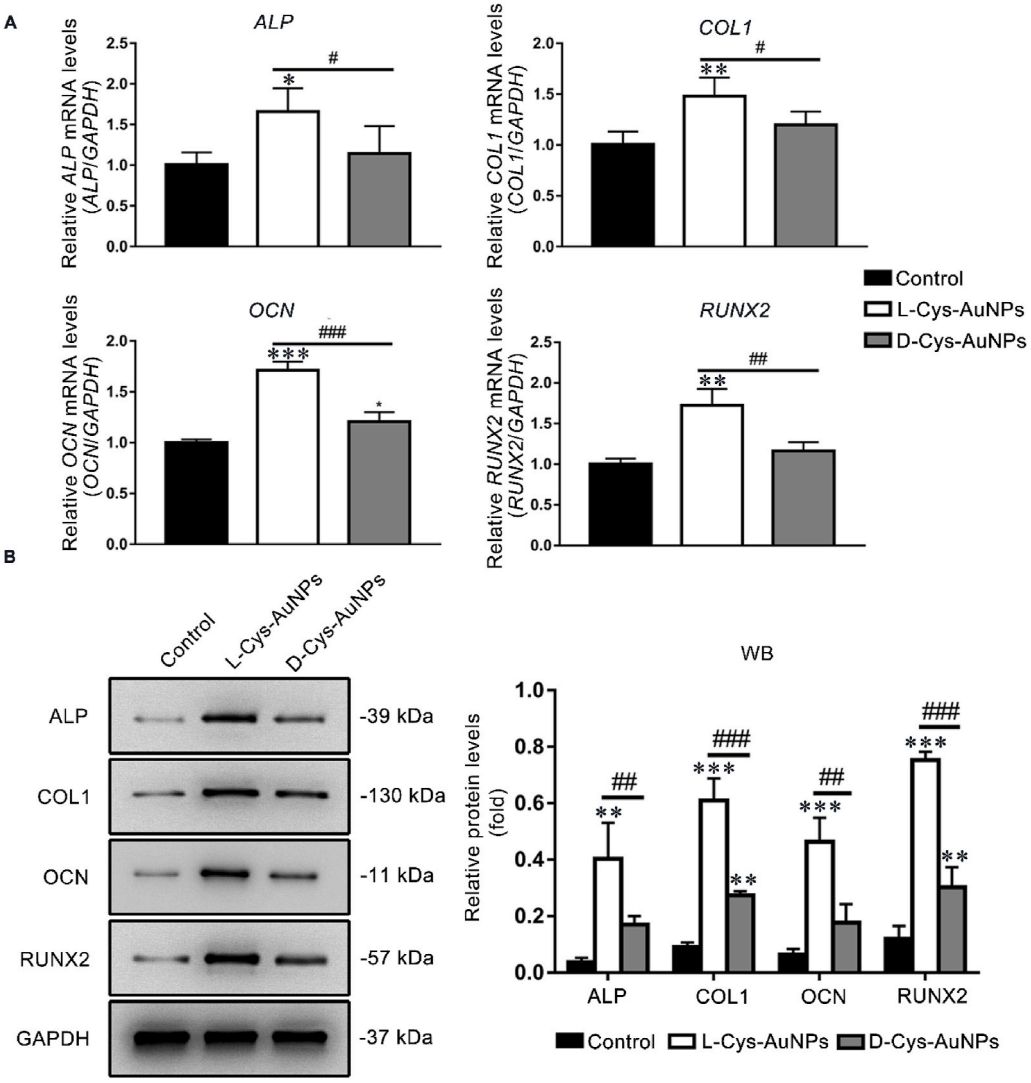

Fig. 3. Effects of L/D-Cys-AuNPs on the osteogenic genes and proteins of hPDLCs cultured with L/D-Cys-AuNPs. (**A**) *ALP, COL1, OCN* and *RUNX2* mRNA levels of L/D-Cys-AuNP-treated hPDLCs on day 5. (**B**) ALP, COL1, OCN and RUNX2 protein levels of L/D-Cys-AuNP-treated hPDLCs on day 7. $^{*}P < 0.05$, $^{**}P < 0.01$, $^{***}P < 0.001$ compared with the control group, $\#P < 0.05$, $\#\#P < 0.01$, $\#\#\#P < 0.001$.

of the following reasons. It was demonstrated that L-enantiomers adsorbed significantly more serum proteins than D-enantiomers [8,41]. In addition, the adsorbed proteins enhanced the cellular uptake of nanoparticles [42,43]. Moreover, L-enantiomers adsorbed more cellular adhesion mediators, such as fibronectin, than D-enantiomers [8,44]. The adhesion mediators may also promote cellular uptake [8] and osteogenesis [44].

Although L/D-Cys-AuNPs could be internalized by hPDLCs, their effects on the cells remain unknown. Because hPDLCs have the potential for osteogenic differentiation, we focused on the effects of L/D-Cys-AuNPs on the osteogenic differentiation of hPDLCs. Early-phase osteogenic differentiation can be assessed by ALP activity [45]. Late-phase osteogenic differentiation is characterized by mineralized nodule deposition, which can be detected by ARS and von Kossa staining [46]. The ALP activity, ARS, and von Kossa staining all indicated that L-Cys-AuNPs had better osteogenic differentiation induction ability on hPDLCs than D-Cys-AuNPs in both the early and late phases of osteogenic differentiation. All tested osteogenic-related mRNA and protein outcomes indicated that the L-Cys-AuNPs had better osteogenic-differentiation-induction ability than D-Cys-AuNPs under our experimental conditions. Although it is consistent with a previous report [8], another study reported a larger proportion of MSCs differentiated into osteoblasts on a D-cysteine glass surface coated with gold after osteogenic co-induction [28]. The cells and co-induction system of our study varies from the two previous ones, so these variations in the results are not surprising. Therefore, further studies are needed to confirm this phenomenon.

In accordance with our study, some studies also found that L-enantiomers promote more stem cell osteogenesis than D-enantiomers [8,44]. One study found that L-enantiomers may activate the P38 mitogen-activated protein kinase pathway through mechanical stress; this may be the possible mechanism of chirality-dependent osteogenic differentiation [8]. Another study ascribes this chiral-dependent differentiation to mechanotransduction events [44]. In our study, both L/D-Cys-AuNPs were observed in autophagosomes, implying that autophagy may be one of the mechanisms through which chiral AuNPs induce the osteogenic differentiation of cells [5]. As AuNPs have been previously shown to induce autophagy [47,48], our study further explored the relationship between the effects of L/D-Cys-AuNPs on hPDLCs and autophagy. *LC3* is an extensively accepted positive autophagy-related marker [49]. From our results, *LC3* mRNA and protein levels in the L-Cys-AuNP-treated group was the highest of the three groups studied. As SQSTM1 is efficiently consumed by autophagic degradation [50], the SQSTM1 protein level is negatively related to

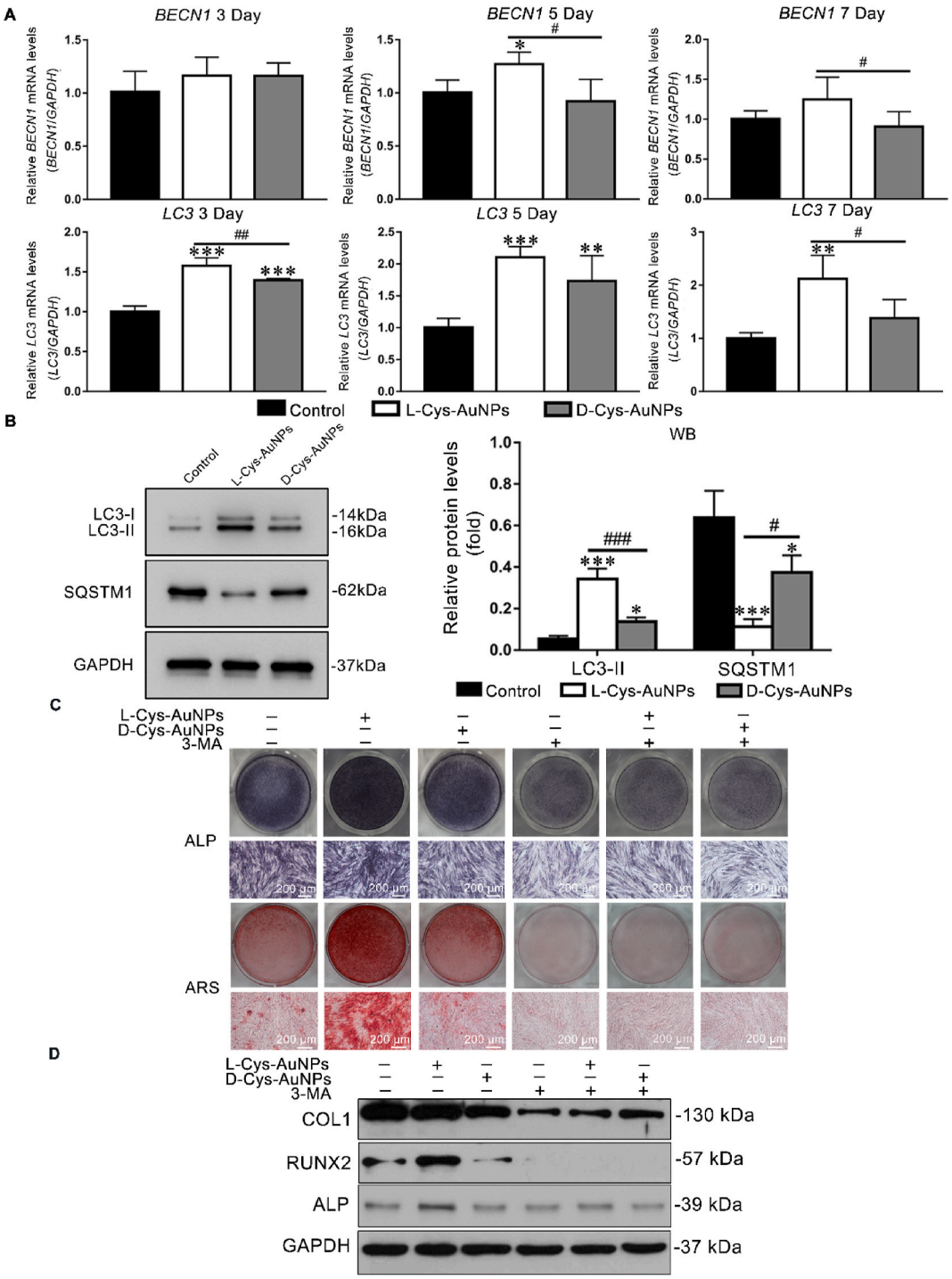

Fig. 4. Effects of L/D-Cys-AuNPs on autophagy genes and proteins of hPDLCs cultured with L/D-Cys-AuNPs. (**A**) *BECN1* and *LC3* mRNA levels of L/D-Cys-AuNP-treated hPDLCs on days 3, 5, and 7. (**B**) LC3-II and SQSTM1 protein levels of L/D-Cys-AuNP-treated hPDLCs on day 7. hPDLCs were then cultured with the autophagy inhibitor 3-MA and L/D-Cys-AuNPs. (**C**) ALP staining on day 7 and ARS staining on day 21. (**D**) COL1, RUNX2, and ALP protein levels of 3-MA and L/D-Cys-AuNP-treated hPDLCs on day 7. $^{*}P < 0.05$, $^{**}P < 0.01$, $^{***}P < 0.001$ compared with the control group, $\#P < 0.05$, $\#\#P < 0.01$, $\#\#\#P < 0.001$.

autophagy. Our results showed that the protein level of SQSTM1 was the lowest in hPDLCs treated with L-Cys-AuNPs. Collectively, our results suggested that the L-Cys-AuNP-treated group resulted in the highest autophagy of the three groups investigated.

The *in vitro* studies suggested that the L-Cys-AuNPs had a more pronounced effect on the osteogenesis of hPDLCs than the D-Cys-AuNPs. This effect could be achieved by modulating autophagy. Therefore, L-Cys-AuNPs could have clinical potential for periodontal regeneration. Based on the *in vitro* study presented here, hPDLCs coupled with L/D-Cys-AuNPs have the potential to generate a better outcome for periodontal regeneration. SD rats were used in this study as an effective strain of an outbred multipurpose breed of albino rat used extensively in dental-related medical research studies [37,51]. Rat periodontal-fenestration-defects that would not heal within 4 weeks on their own were established through the methods described in the literature [37,38,51]. L-Cys-AuNPs promoted the rat periodontal regeneration, and its effects were better than those observed for the D-Cys-AuNPs.

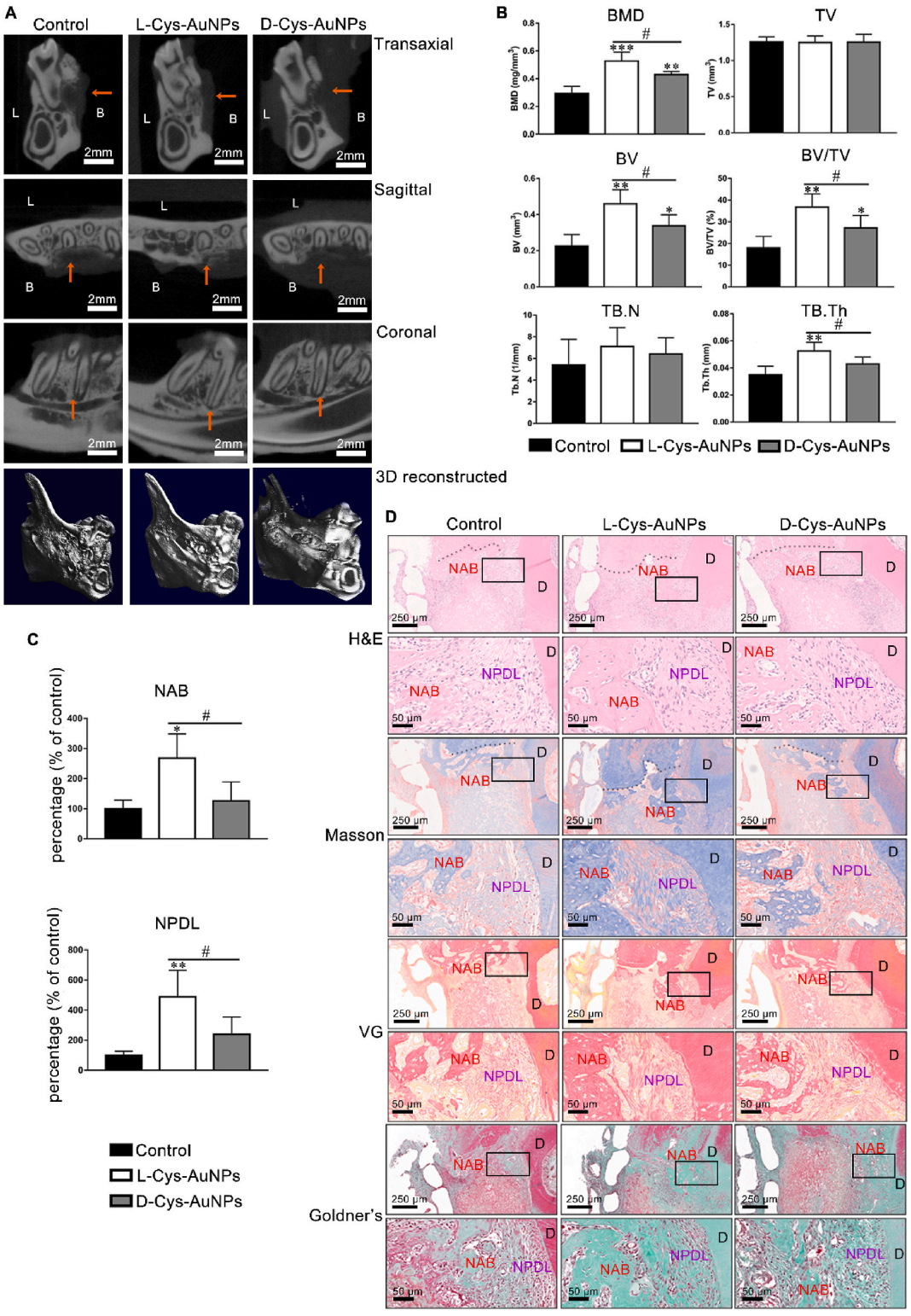

Fig. 5. L-Cys-AuNPs showed the best *in-vivo* periodontal regeneration potential in the rat periodontal-fenestration-defect model. hPDLCs were seeded onto a resorbable collagen membrane and cultured with L/D-Cys-AuNPs. The treated cell-membrane compounds were placed into the rat periodontal-fenestration-defect models and embedded for 21 days. (**A**) μCT images of the mandibular first molars (B means buccal and L means lingual). (**B**) Bone-related parameters (BMD, TV, BV, BV/TV, Tb.Th, and Tb.N) reported by μCT. (**C**) Quantification of NAB and NPDL. (**D**) The representative H&E, Masson, VG, and Goldner's staining images (D means dentin, NAB means newly-formed alveolar bones, and NPDL means newly-formed periodontal ligaments). $^{*}P < 0.05$, $^{**}P < 0.01$, $^{***}P < 0.001$ compared with the control group, $\#P < 0.05$.

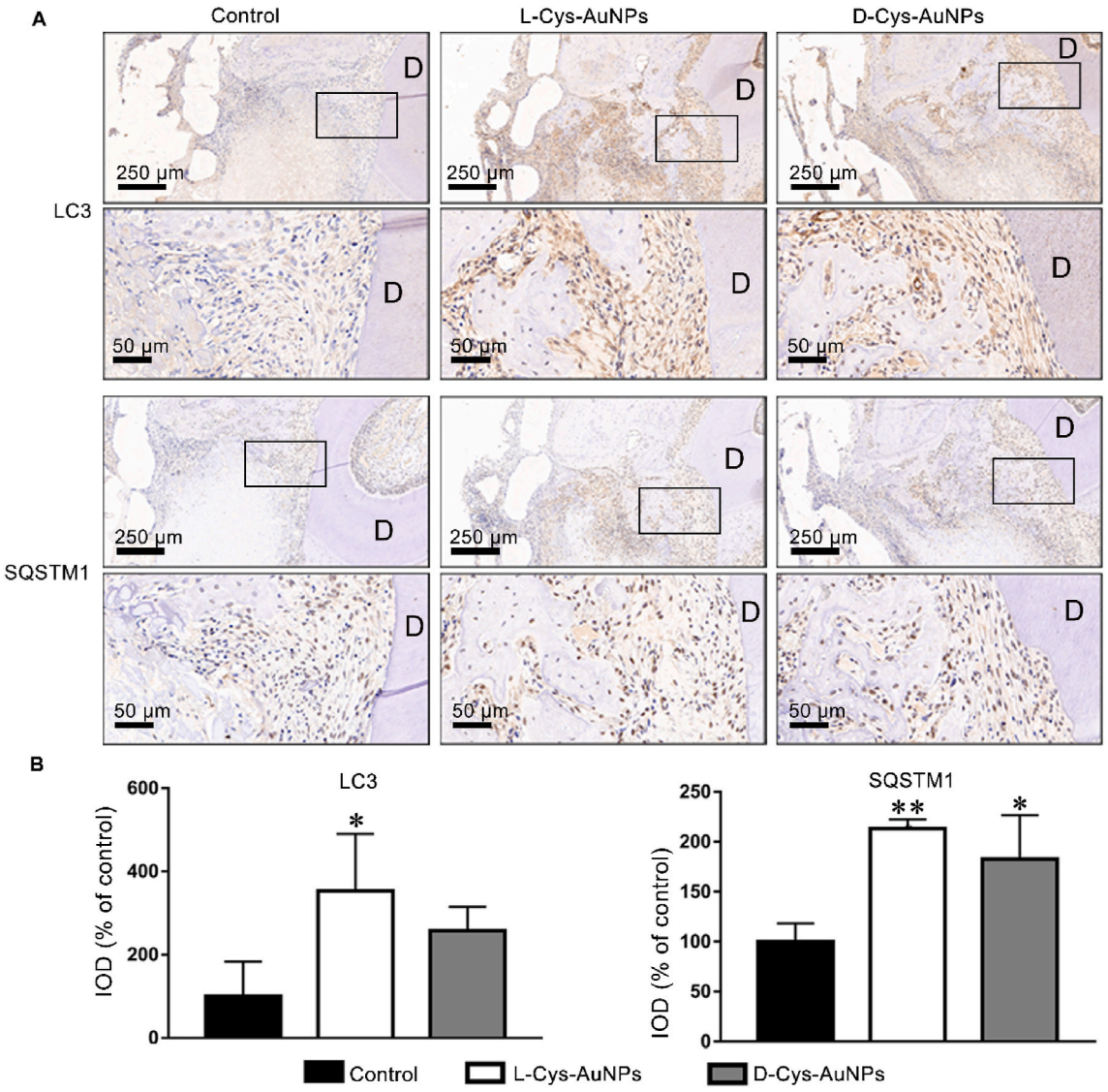

Fig. 6. L/D-Cys-AuNP-modulated autophagy in the rat periodontal-fenestration-defect model. hPDLCs were seeded onto a resorbable collagen membrane and cultured with L/D-Cys-AuNPs. The treated cell-membrane compounds were placed into the rat periodontal-fenestration-defect models and cultured for 21 days. (**A**) Expression of LC3 and SQSTM1 protein levels in the periodontal tissue of the mandibular first molars (D means dentin). (**B**) Quantification of LC3 and SQSTM1. $^{*}P < 0.05$, $^{**}P < 0.01$ compared with the control group.

To the best of our knowledge, our study is the first to explore the chiral effect on hPDLCs. Our chiral AuNP culture system accurately mimics the biophysical environment of natural three-dimensional cell culture and is easy to apply for extensive applications. In addition, it can enter the cell and interact with cell organs and proteins to promote osteogenesis.

To further develop the application of AuNPs in nanomedicine, it is imperative to note the limitations of our study. First, the mechanism and pathway of the effects of AuNPs on osteogenesis through autophagy require extensive investigation. Second, large animals should be used for a more robust experimentation. Third, a variety of chiral AuNPs should be constructed for further study. The working mechanism of chirality and its influence on the cellular internalization of nanoparticles should be carefully explored.

5. Conclusions

This study shows the enhanced effectiveness of L-Cys-AuNPs compared to D-Cys-AuNPs in promoting osteogenic differentiation in hPDLCs and periodontal regeneration in a rat periodontal-defect model. These findings indicate that surface chirality should be considered for the development of functional biomaterials to guide cell differentiation and tissue regeneration. Hence, L-Cys-AuNPs are an attractive and promising candidate for periodontal tissue engineering in the future. Furthermore, the influence of surface chirality requires detailed investigation for the rational designing of novel biomedical nanomaterials. Our study may open a new way for the development of chiral-molecule-modified nanoparticles for biomedical applications.

Ethics statement

All the animal experiments obeyed the rules of the National Institutes of Health guide for the care and use of Laboratory animals and were approved by the Animal Ethics Committee of Nanjing University. We confirm authors' compliance with all relevant ethical regulations.

CRediT authorship contribution statement

Shuang Zhang: Conceptualization, Data curation, Investigation, Methodology, Project administration, Resources, Validation,

Visualization, Writing – original draft. **Hong Zhou:** Funding acquisition, Visualization, Writing – review & editing. **Na Kong:** Methodology, Project administration, Resources, Writing – review & editing. **Zezheng Wang:** Data curation, Formal analysis, Methodology, Project administration, Writing – review & editing. **Huangmei Fu:** Methodology, Project administration, Resources, Writing – review & editing. **Yangheng Zhang:** Methodology, Writing – review & editing. **Yin Xiao:** Supervision, Validation, Writing – review & editing. **Wenrong Yang:** Conceptualization, Resources, Supervision, Validation, Funding acquisition, Writing – review & editing. **Fuhua Yan:** Conceptualization, Data curation, Funding acquisition, Supervision, Validation, Visualization, Writing – review & editing.

Declaration of competing interest

None.

Acknowledgements

This work was supported by The National Natural Science Foundation Project [grant numbers 81771078, 81570982, 21675074, 21675075], Jiangsu Provincial Medical Innovation Team, The Project of Invigorating Health Care through Science, Technology and Education [grant number CXTDB2017014], the Nanjing Clinical Research Center for Oral Diseases [grant number 2019060009], and The Natural Science Foundation of Shandong Province (ZR2018ZC0231). The authors thank Central Laboratory of Stomatology, Nanjing Stomatological Hospital, Medical School of Nanjing University.

References

[1] B.L. Pihlstrom, B.S. Michalowicz, N.W. Johnson, Periodontal diseases, Lancet 366 (9499) (2005) 1809–1820.
[2] S. Offenbacher, Y. Jiao, S.J. Kim, J. Marchesan, K.L. Moss, L. Jing, K. Divaris, S. Bencharit, C.S. Agler, T. Morelli, S. Zhang, L. Sun, W.T. Seaman, D. Cowley, S. P. Barros, J.D. Beck, M. Munz, A.S. Schaefer, K.E. North, GWAS for Interleukin-1beta levels in gingival crevicular fluid identifies IL37 variants in periodontal inflammation, Nat. Commun. 9 (1) (2018) 3686.
[3] B.-M. Seo, M. Miura, S. Gronthos, P. Mark Bartold, S. Batouli, J. Brahim, M. Young, P. Gehron Robey, C.Y. Wang, S. Shi, Investigation of multipotent postnatal stem cells from human periodontal ligament, Lancet 364 (9429) (2004) 149–155.
[4] J. Zhou, Y. Zhang, L. Li, H. Fu, W. Yang, F. Yan, Human beta-defensin 3-combined gold nanoparticles for enhancement of osteogenic differentiation of human periodontal ligament cells in inflammatory microenvironments, Int. J. Nanomed. 13 (2018) 555–567.
[5] Y. Zhang, N. Kong, Y. Zhang, W. Yang, F. Yan, Size-dependent effects of gold nanoparticles on osteogenic differentiation of human periodontal ligament progenitor cells, Theranostics 7 (5) (2017) 1214–1224.
[6] Z. Xiang, K. Wang, W. Zhang, S.W. Teh, A. Peli, P.L. Mok, A. Higuchi, S. Suresh Kumar, Gold nanoparticles inducing osteogenic differentiation of stem cells: a review, J. Cluster Sci. 29 (1) (2018) 1–7.
[7] M.G. Donato, J. Hernandez, A. Mazzulla, C. Provenzano, R. Saija, R. Sayed, S. Vasi, A. Magazzu, P. Pagliusi, R. Bartolino, P.G. Gucciardi, O.M. Marago, G. Cipparrone, Polarization-dependent optomechanics mediated by chiral microresonators, Nat. Commun. 5 (2014) 3656.
[8] J. Deng, H. Zheng, X. Zheng, M. Yao, Z. Li, C. Gao, Gold nanoparticles with surface-anchored chiral poly(acryloyl-L(D)-valine) induce differential response on mesenchymal stem cell osteogenesis, Nano Res. 9 (12) (2016) 3683–3694.
[9] K. Ariga, T. Mori, T. Kitao, T. Uemura, Supramolecular chiral nanoarchitectonics, Adv. Mater. 32 (41) (2020) 1905657.
[10] W. Ma, L. Xu, A. de Moura, X. Wu, H. Kuang, C. Xu, N. Kotov, Chiral inorganic nanostructures, Chem. Rev. 117 (12) (2017) 8041–8093.
[11] C. Liu, L. Zhang, W. Chen, F. Yang, Chiral spin density wave and d+id superconductivity in the magic-angle-twisted bilayer graphene, Phys. Rev. Lett. 121 (21) (2018) 217001.
[12] P. Lodahl, S. Mahmoodian, S. Stobbe, A. Rauschenbeutel, P. Schneeweiss, J. Volz, H. Pichler, P. Zoller, Chiral quantum optics, Nature 541 (7638) (2017) 473–480.
[13] K. Takaishi, M. Yasui, T. Ema, Binaphthyl-bipyridyl cyclic dyads as a chiroptical switch, J. Am. Chem. Soc. 140 (16) (2018) 5334–5338.
[14] T. Saint-Denis, R. Zhu, G. Chen, Q. Wu, J. Yu, Enantioselective C(sp)–H bond activation by chiral transition metal catalysts, Science (New York, N.Y.) 359 (6377) (2018).
[15] J. Labuta, S. Ishihara, T. Šikorský, Z. Futera, A. Shundo, L. Hanyková, J. Burda, K. Ariga, J. Hill, NMR spectroscopic detection of chirality and enantiopurity in referenced systems without formation of diastereomers, Nat. Commun. 4 (2013) 2188.
[16] M. Solomon, A. Saleh, L. Poulikakos, J. Abendroth, L. Tadesse, J. Dionne, Nanophotonic platforms for chiral sensing and separation, Acc. Chem. Res. 53 (3) (2020) 588–598.
[17] J. Kumar, L.M. Liz-Marzán, Recent advances in chiral plasmonics — towards biomedical applications, Bull. Chem. Soc. Jpn. 92 (1) (2019) 30–37.
[18] M. Sun, L. Xu, J. Bahng, H. Kuang, S. Alben, N. Kotov, C. Xu, Intracellular localization of nanoparticle dimers by chirality reversal, Nat. Commun. 8 (1) (2017) 1847.
[19] L. Xu, Y. Gao, H. Kuang, L. Liz-Marzán, C. Xu, MicroRNA-directed intracellular self-assembly of chiral nanorod dimers, Angew. Chem. 57 (33) (2018) 10544–10548.
[20] J. Kumar, H. Eraña, E. López-Martínez, N. Claes, V. Martín, D. Solís, S. Bals, A. Cortajarena, J. Castilla, L. Liz-Marzán, Detection of amyloid fibrils in Parkinson's disease using plasmonic chirality, Proc. Natl. Acad. Sci. U.S.A. 115 (13) (2018) 3225–3230.
[21] F. Gao, M. Sun, W. Ma, X. Wu, L. Liu, H. Kuang, C. Xu, A singlet oxygen generating agent by chirality-dependent plasmonic shell-satellite nanoassembly, Adv. Mater. (Deerfield Beach, Fla.) 29 (18) (2017).
[22] N. Xu, G. Chen, H. Liu, Antioxidative categorization of twenty amino acids based on experimental evaluation, Molecules 22 (12) (2017).
[23] B. Thirumalraj, N. Dhenadhayalan, S.-M. Chen, Y.-J. Liu, T.-W. Chen, P.-H. Liang, K.-C. Lin, Highly sensitive fluorogenic sensing of L-Cysteine in live cells using gelatin-stabilized gold nanoparticles decorated graphene nanosheets, Sensor. Actuator. B Chem. 259 (2018) 339–346.
[24] S.D. Cen, W.B. Yu, M.M. Ren, L.J. Chen, C.F. Sun, Z.L. Ye, H. Deng, R.D. Hu, Endogenous hydrogen sulfide is involved in osteogenic differentiation in human periodontal ligament cells, Arch. Oral Biol. 68 (2016) 1–8.
[25] N.R. Jana, X. Peng, Single-phase and gram-scale routes toward nearly monodisperse Au and other noble metal nanocrystals, J. Am. Chem. Soc. 125 (47) (2003) 14280–14281.
[26] F. Yang, K. Na, X.A. Conlan, H. Wang, C.J. Barrow, F. Yan, J. Guo, W. Yang, Electrochemical evidences of chiral molecule recognition using L/D -cysteine modified gold electrodes, Electrochim. Acta 237 (2017) 22–28.
[27] Y. Zhang, J. Liu, D. Li, X. Dai, F. Yan, X.A. Conlan, R. Zhou, C.J. Barrow, J. He, X. Wang, W. Yang, Self-Assembled core-satellite gold nanoparticle networks for ultrasensitive detection of chiral molecules by recognition tunneling current, ACS Nano 10 (5) (2016) 5096–5103.
[28] X. Yao, Y. Hu, B. Cao, R. Peng, J. Ding, Effects of surface molecular chirality on adhesion and differentiation of stem cells, Biomaterials 34 (36) (2013) 9001–9009.
[29] A. Pielesz, D. Binias, R. Bobinski, E. Sarna, J. Paluch, W. Waksmanska, The role of topically applied l-ascorbic acid in ex-vivo examination of burn-injured human skin, Spectrochim. Acta Mol. Biomol. Spectrosc. 185 (2017) 279–285.
[30] A. Pantovic, A. Krstic, K. Janjetovic, J. Kocic, L. Harhaji-Trajkovic, D. Bugarski, V. Trajkovic, Coordinated time-dependent modulation of AMPK/Akt/mTOR signaling and autophagy controls osteogenic differentiation of human mesenchymal stem cells, Bone 52 (1) (2013) 524–531.
[31] Z. Zhou, G. Shi, X. Zheng, S. Jiang, L. Jiang, Autophagy activation facilitates mechanical stimulation-promoted osteoblast differentiation and ameliorates hindlimb unloading-induced bone loss, Biochem. Biophys. Res. Commun. 498 (3) (2018) 667–673.
[32] F. Liu, F. Fang, H. Yuan, D. Yang, Y. Chen, L. Williams, S.A. Goldstein, P. H. Krebsbach, J.L. Guan, Suppression of autophagy by FIP200 deletion leads to osteopenia in mice through the inhibition of osteoblast terminal differentiation, J. Bone Miner. Res. 28 (11) (2013) 2414–2430.
[33] M. Sun, T. Hao, X. Li, A. Qu, L. Xu, C. Hao, C. Xu, H. Kuang, Direct observation of selective autophagy induction in cells and tissues by self-assembled chiral nanodevice, Nat. Commun. 9 (1) (2018) 4494.
[34] Z. Weng, H. Wang, J. Vongsvivut, R. Li, A.M. Glushenkov, J. He, Y. Chen, C. J. Barrow, W. Yang, Self-assembly of core-satellite gold nanoparticles for colorimetric detection of copper ions, Anal. Chim. Acta 803 (2013) 128–134.
[35] W. Haiss, N.T. Thanh, J. Aveyard, D.G. Fernig, Determination of size and concentration of gold nanoparticles from UV-vis spectra, Anal. Chem. 79 (11) (2007) 4215–4221.
[36] A. Foroushani, Y. Zhang, D. Li, M. Mathesh, H. Wang, F. Yan, C.J. Barrow, J. He, W. Yang, Tunnelling current recognition through core-satellite gold nanoparticles for ultrasensitive detection of copper ions, Chem. Commun. (Camb) 51 (14) (2015) 2921–2924.
[37] P. Han, S. Ivanovski, R. Crawford, Y. Xiao, Activation of the canonical wnt signaling pathway induces cementum regeneration, J. Bone Miner. Res. 30 (7) (2015) 1160–1174.
[38] C. Ni, J. Zhou, N. Kong, T. Bian, Y. Zhang, X. Huang, Y. Xiao, W. Yang, F. Yan, Gold nanoparticles modulate the crosstalk between macrophages and periodontal ligament cells for periodontitis treatment, Biomaterials 206 (2019) 115–132.
[39] K. You, Y. Huang, M.C. Zhang, J. Hao, Control and prevention of myocardial fibrosis using Pyk2-related non-kinase, Int. J. Clin. Exp. Med. 8 (10) (2015) 18284–18292.
[40] C. Peng, X. Gao, J. Xu, B. Du, X. Ning, S. Tang, R.M. Bachoo, M. Yu, W.P. Ge, J. Zheng, Targeting orthotopic gliomas with renal-clearable luminescent gold nanoparticles, Nano Res. 10 (4) (2017) 1366–1376.
[41] J. Deng, S. Wu, M. Yao, C. Gao, Surface-anchored poly(acryloyl-L(D)-valine) with enhanced chirality-selective effect on cellular uptake of gold nanoparticles, Sci. Rep. 6 (2016) 31595.
[42] B. Pelaz, P. del Pino, P. Maffre, R. Hartmann, M. Gallego, S. Rivera-Fernandez, J. M. de la Fuente, G.U. Nienhaus, W.J. Parak, Surface functionalization of nanoparticles with polyethylene glycol: effects on protein adsorption and cellular uptake, ACS Nano 9 (7) (2015) 6996–7008.

[43] M.P. Calatayud, B. Sanz, V. Raffa, C. Riggio, M.R. Ibarra, G.F. Goya, The effect of surface charge of functionalized Fe3O4 nanoparticles on protein adsorption and cell uptake, Biomaterials 35 (24) (2014) 6389–6399.
[44] Y. Wei, S. Jiang, M. Si, X. Zhang, J. Liu, Z. Wang, C. Cao, J. Huang, H. Huang, L. Chen, S. Wang, C. Feng, X. Deng, L. Jiang, Chirality controls mesenchymal stem cell lineage diversification through mechanoresponses, Adv. Mater. 31 (16) (2019), e1900582.
[45] L. Zhao, L. Liu, Z. Wu, Y. Zhang, P.K. Chu, Effects of micropitted/nanotubular titania topographies on bone mesenchymal stem cell osteogenic differentiation, Biomaterials 33 (9) (2012) 2629–2641.
[46] S.H. Shin, J.J. Yoo, H.N. Kim, J. Nam, H.J. Kim, Enhanced cellular responses of human bone marrow stromal cells cultured on pretreated surface with allogenic platelet-rich plasma, Connect. Tissue Res. 53 (4) (2012) 318–326.
[47] L. Yuan, F. Zhang, X. Qi, Y. Yang, C. Yan, J. Jiang, J. Deng, Chiral polymer modified nanoparticles selectively induce autophagy of cancer cells for tumor ablation, J. Nanobiotechnol. 16 (1) (2018) 55.
[48] Q. Wang, Y. Zhou, R. Fu, Y. Zhu, B. Song, Y. Zhong, S. Wu, Y. Shi, Y. Wu, Y. Su, H. Zhang, Y. He, Distinct autophagy-inducing abilities of similar-sized nanoparticles in cell culture and live C. elegans, Nanoscale 10 (48) (2018) 23059–23069.
[49] C. Grose, E.M. Buckingham, J.E. Carpenter, J.P. Kunkel, Varicella-zoster virus infectious cycle: ER stress, autophagic flux, and amphisome-mediated trafficking, Pathogens 5 (4) (2016).
[50] N. Mizushima, T. Yoshimori, B. Levine, Methods in mammalian autophagy research, Cell 140 (3) (2010) 313–326.
[51] C. Chen, H. Li, J. Jiang, Q. Zhang, F. Yan, Inhibiting PHD2 in bone marrow mesenchymal stem cells via lentiviral vector-mediated RNA interference facilitates the repair of periodontal tissue defects in SD rats, Oncotarget 8 (42) (2017) 72676–72699.